J. Fluid Mech. (2001), *vol.* 442, *pp.* 67–88. Printed in the United Kingdom

Response of a circular cylinder wake to superharmonic excitation

By SEUNG-JIN BAEK, SANG BONG LEE AND HYUNG JIN SUNG†

Department of Mechanical Engineering, Korea Advanced Institute of Science and Technology, 373-1, Kusong-dong, Yusong-ku, Taejon, 305-701, Korea

(Received 10 May 2000 and in revised form 22 February 2001)

A systematic numerical analysis is performed for superharmonic excitations in a wake where a circular cylinder is rotationally oscillated in time. Emphasis is placed on identifying the secondary and tertiary lock-on in the forced wakes. The frequency responses are scrutinized by measuring the lift coefficient (C_L). A direct numerical simulation has been conducted to portray the unsteady dynamics of wake flows behind a circular cylinder. The Reynolds number based on the diameter is $Re = 106$, and the forcing magnitude is $0.10 \leqslant \Omega_{max} \leqslant 0.40$. The tertiary lock-on is observed, where the shedding frequency (St_0) is one third of the forcing frequency (S_f), i.e. the $1/3$ subharmonic lock-on. The phase shift of C_L with respect to the forcing frequency is observed. It is similar to that of the primary lock-on. However, in the secondary superharmonic excitation, modulated oscillations are observed, i.e. the lock-on does not exist. As Ω_{max} increases, St_0 is gradually shifted from the natural shedding frequency (St_0^*) to lower values. The magnitudes and phases of S_f and St_0 are analysed by the phase diagram. The vorticity contours are employed to examine the vortex formation mode against the forcing conditions.

1. Introduction

Much work has been carried out on the near-wake flow structure behind a circular cylinder subjected to controlled forcings. These studies were performed to understand the interrelation between the near-wake flow structure and the forcing on the body. Several different types of forcing were applied to the cylinder, and the overall wake responses were similar: transverse oscillation (Ongoren & Rockwell 1988; Hover, Techet & Triantafyllou 1998; Techet, Hover & Triantafyllou 1998; Blackburn & Henderson 1999), alternate suction and blowing (Williams, Mansy & Amato 1992; Park, Ladd & Hendricks 1994) and rotational oscillation (Tokumaru & Dimotakis 1991; Filler, Marston & Mih 1991; Baek & Sung 1998, 2000; Dennis, Nguyen & Kocabiyik 2000), to name a few. Reviews of the controlled flows are compiled in Bearman (1984), Griffin & Hall (1991) and Rockwell (1998). With no external forcings, the flow exhibits self-excited oscillations, i.e. the Kármán vortices are shed to the rear of the cylinder. In the forced wake flows, however, vortex shedding is entrained by the cylinder motion, hence the vortex shedding frequency changes to match the cylinder forcing frequency. This is the 'lock-on' phenomenon, where the self-excited oscillation synchronizes with the forcing frequency provided that the two frequencies are not too different.

† Author for correspondence: e-mail: hjsung@kaist.ac.kr.

If the difference in the two frequencies is large enough, a quasi-periodic or chaotic oscillation may occur (Baek & Sung 2000). However, the entrainment of frequency still occurs when a ratio of the forcing frequency to the natural frequency of the self-excited oscillation is in the neighbourhood of an integer or a fraction. Under this condition, the natural frequency is entrained by a frequency which is an integer multiple or submultiple of the forcing frequency. Such an entrainment is called 'superharmonic' or 'subharmonic' lock-on, respectively, in contrast with the aforestated harmonic entrainment, i.e. the primary lock-on.

A considerable amount of literature concerning the primary lock-on is available (Koopman 1967; Ongoren & Rockwell 1988; Karniadakis & Triantafyllou 1989; Gu, Chyu & Rockwell 1994; Baek & Sung 1998; Blackburn & Henderson 1999). However, a literature survey reveals that there are not many reports on the occurrence of superharmonic or subharmonic lock-on. A few experimental studies have been performed on the subharmonic lock-on (Stansby 1976; Ongoren & Rockwell 1988). When the forcing frequency is in the vicinity of two or three times the natural shedding frequency, the vortex shedding can be entrained at a half or a third of the forcing frequency. These entrainments at a half or a third of the forcing frequency are referred to as the 'secondary' or 'tertiary' lock-on, respectively. The available published data for the existence of these entrainments have been inconclusive. Stansby (1976) showed the existence of the secondary and tertiary lock-on region. However, the secondary lock-on was observed in a very small range of the forcing frequency. A numerical simulation of the superharmonic excitation was performed by El-Refaee (1995). He found no evidence of the secondary lock-on, although the tertiary lock-on exists.

One way to deal with these discrepancies is to re-evaluate the subharmonic lock-on in a systematic way. The objective of the present study is to analyse the response of wakes to the superharmonic excitation. Toward this end, a series of direct numerical simulations are conducted. The range of forcing frequency covers up to two and three times the natural shedding frequency. Emphasis is placed on the question of whether the subharmonic lock-on exists in the superharmonic excitation. The frequency response is analysed based on the phase diagram, which provides the information about its magnitude and phase. The behaviour of the controlled near-wakes is examined by measuring the lift coefficient (C_L). The power spectral density plots and the vorticity contours are employed to analyse the forced wakes behind a circular cylinder. The present study represents an extension of the previous efforts (Baek & Sung 1998, 2000), where the rotationally oscillating forcing frequency was in the neighbourhood of the natural shedding frequency. Baek & Sung (1998) observed the phase switching phenomena, and they classified the vortex formation patterns in the primary lock-on region. The quasi-periodicity in the exterior region of the primary lock-on was scrutinized by Baek & Sung (2000). It was found that, after the shedding frequency is bifurcated at the boundary of lock-on, one frequency follows the forcing frequency and the other gradually converges to the natural shredding frequency.

A direct numerical simulation is made in the present study to portray the unsteady dynamics of wake flows behind a circular cylinder. The Reynolds number based on the diameter (D) is fixed at $Re = 106$, and the vortex shedding flow is assumed to be two-dimensional (Williamson 1996). Excitation is given by the rotational oscillation of a circular cylinder. The natural shedding frequency is $St_0^* = 0.168$ and the forcing frequency (S_f) varies in the vicinity of $2St_0^* = 0.336$ and $3St_0^* = 0.504$. The maximum rotation velocity (Ω_{max}) is in the range $0.10 \leqslant \Omega_{max} \leqslant 0.40$.

2. Numerical method

The non-dimensional governing equations for unsteady incompressible flow are

$$\frac{\partial u_i}{\partial t} + \frac{\partial}{\partial x_j} u_i u_j = -\frac{\partial p}{\partial x_i} + \frac{1}{Re} \frac{\partial}{\partial x_j} \frac{\partial}{\partial x_j} u_i, \tag{2.1}$$

$$\frac{\partial u_i}{\partial x_i} = 0, \tag{2.2}$$

where x_i is the Cartesian coordinates and u_i is the velocity component. The free-stream velocity U_∞ and the cylinder diameter D are used in non-dimensionalization. The Reynolds number is defined as $Re = U_\infty D/\nu$, where ν is the kinematic viscosity.

To simulate wake flows behind a cylinder, it is useful to transform the governing equations (2.1) and (2.2) into the generalized coordinates y^i (Choi, Moin & Kim 1992). The velocity components u_i are transformed into the volume fluxes across the faces of the cell q^i. The formulation in terms of the contravariant velocity components leads to discretized equations in conjunction with the staggered variable configuration. The resulting pressure Poisson equation is solved, where the discretized mass conservation is satisfied.

A fully implicit, fractional-step method composed of four-step time advancement is used to solve the governing equations (Choi , Moin & Kim 1993). The fractional step, or time-split method, is an approximate technique for the evolution equations based on the decomposition of the operators. In applying this method to the Navier–Stokes equations, we can interpret the role of pressure in the momentum equations as a projection operator, which projects an arbitrary vector field into a divergence-free vector. In Cartesian coordinates, these four steps are

$$\frac{\hat{u}_i - u_i^n}{\Delta t} + \frac{1}{2} \frac{\partial}{\partial x_j} (\hat{u}_i \hat{u}_j + u_i^n u_j^n) = -\frac{\partial p^n}{\partial x_i} + \frac{1}{2} \frac{1}{Re} \frac{\partial}{\partial x_j} \frac{\partial}{\partial x_j} (\hat{u}_i + u_i^n), \tag{2.3}$$

$$\frac{\check{u}_i - \hat{u}_i}{\Delta t} = \frac{\partial p^n}{\partial x_i}, \tag{2.4}$$

$$\frac{\partial}{\partial x_i} \frac{\partial p^{n+1}}{\partial x_i} = \frac{1}{\Delta t} \frac{\partial \check{u}_i}{\partial x_i}, \tag{2.5}$$

$$\frac{u_i^{n+1} - \check{u}_i}{\Delta t} = -\frac{\partial p^{n+1}}{\partial x_i}. \tag{2.6}$$

A second-order central difference scheme is used for the spatial derivatives and a Crank–Nicolson method is employed in time advancement. Substitution of equations (2.4) and (2.6) into equation (2.3) indicates that the present scheme is second-order accurate in time. The discretized nonlinear momentum equations are solved by using a Newton iterative method. Solving the Poisson equation for p satisfies the continuity equation. In this computation, equations (2.3)–(2.6) are also transformed from Cartesian coordinates to the generalized coordinate.

A flow configuration of the present rotational oscillation is shown in figure 1. A C-mesh is used for the present simulation. This type of mesh is suitable for simulating wake flows since higher streamwise resolution can be had in the wake region. The use of a C-mesh simplifies the application of outflow boundary conditions. The outflow boundaries are located at $40D$ and the transverse boundaries are at $50D$, which corresponds to $(x, y) = (449 \times 121)$. A uniform free-stream velocity is prescribed at the inflow and far-field boundaries, and a convective boundary condition is specified

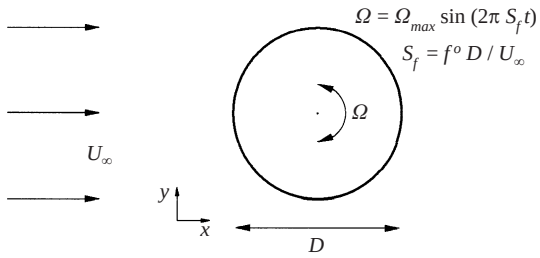

FIGURE 1. Flow configuration of the rotational oscillation.

at the outflow boundary in order to convect the disturbances smoothly out of the computational domain (Pauley, Moin & Reynolds 1990). On the cylinder wall, the periodic rotational oscillation conditions are enforced.

Since the cylinder is rotated sinusoidally in time t^o at a forcing rotational frequency f^o, the non-dimensional cylinder rotation velocity (Ω) is expressed by

$$\Omega = \Omega_{max} \sin(2\pi S_f t), \tag{2.7}$$

where the quantities are non-dimensionalized by adopting the following relations: $t = t^o U_\infty / D$ and $S_f = f^o D / U_\infty$. Here, the superscript 'o' denotes the dimensional counterpart. The maximum rotation velocity Ω_{max} varies from 10% to 40% of the free-stream velocity, i.e. $0.10 \leqslant \Omega_{max} \leqslant 0.40$. Based on equation (2.7), the counter-clockwise rotation occurs in the time 0 to $0.5T$, and the clockwise rotation from $0.5T$ to T. Accordingly, the counterclockwise rotation velocity is maximum at $0.25T$ and the clockwise rotation velocity is maximum at $0.75T$. Here, T denotes the non-dimensional forcing period, i.e. $U_\infty / f^o D = 1/S_f$.

The cylinder wake at $Re = 106$ has a two-dimensional periodic laminar vortex shedding. The $St_0^* - Re$ formulae in the range $50 \leqslant Re \leqslant 160$, pertinent to parallel vortex shedding, were obtained by Williamson (1989) and Fey, König & Eckelmann (1998). The predicted value by the present simulation at $Re = 106$ is $St_0^* = 0.168$, which is in agreement with the results of Williamson (1989) and Fey *et al.* (1998). Details regarding the flow configuration, boundary conditions, grid resolution and other numerical procedures are compiled in Baek & Sung (1998, 2000).

3. Response to the tertiary superharmonic excitation

As mentioned earlier, Stansby (1976) observed the primary and tertiary lock-on for the cylinder vibration at $Re \approx 7000$ and 9200. However, the secondary lock-on occurred in only a very small range of the forcing frequency (S_f). El-Refaee (1995) performed a boundary-element numerical simulation at $Re = 1500$ and 3000, where a circular cylinder was rotationally oscillated. The primary and tertiary lock-on regions were observed, whereas no evidence of the secondary lock-on was found. These two studies corroborated the existence of the tertiary region. However, the existence of the secondary lock-on appears to depend on the forcing conditions. In order to ascertain these discrepancies, the tertiary lock-on is examined first in the present study, where the forcing frequency (S_f) is set at about three times the natural shedding frequency (St_0^*).

The forcing frequency $S_f = 0.504$ is chosen, which is three times the natural shedding frequency $St_0^* = 0.168$. Four forcing amplitudes are applied, $\Omega_{max} = 0.10$, 0.20, 0.30 and 0.40. Time histories of the lift coefficient (C_L) in six forcing periods

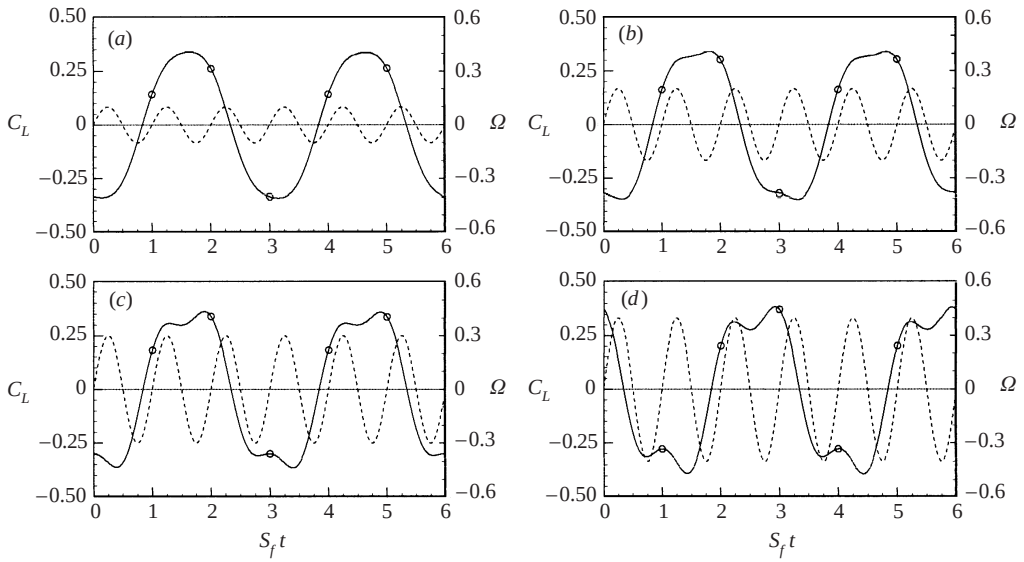

FIGURE 2. Time histories of $C_L(\theta)$ for the tertiary superharmonic excitation ($S_f = 3St_0^* = 0.504$). (*a*) $\Omega_{max} = 0.10$; (*b*) 0.20; (*c*) 0.30; (*d*) 0.40.

($0 \leqslant S_f t \leqslant 6$) are shown in figure 2 by solid lines. The dotted line represents the rotating circumferential velocity (Ω). After a transient stage, the tertiary lock-on is observed in all cases. The small points on the solid line denote the C_L values at the instant when the counterclockwise rotation starts, i.e. the forcing phase $\theta(= 2\pi S_f t)$ is zero ($\theta = 2n\pi$). In figure 2, C_L returns exactly to the original value after three forcing periods. This is a manifestation of the 1/3 subharmonic lock-on. In figure 2(a, b), C_L changes monotonically from peak to peak. However, a closer inspection of figure 2(c, d) indicates that C_L increases again after a small decrease and then becomes a maximum, i.e. two local maximum peaks are seen.

Since the tertiary superharmonic excitations are perturbed, C_L can be decomposed into the forcing frequency (S_f) and its subsequent shedding frequency ($\frac{1}{3}S_f$) terms. In the case of tertiary lock-on, C_L can be expressed as

$$\begin{aligned} C_L(t) &= A_f \cos(2\pi S_f t - \phi_f) + A_{1/3} \cos(2\pi \tfrac{1}{3} S_f t - \tfrac{1}{3}\phi_{1/3}) \\ &= A_f \cos(\theta - \phi_f) + A_{1/3} \cos(\tfrac{1}{3}\theta - \tfrac{1}{3}\phi_{1/3}), \end{aligned} \tag{3.1}$$

where A_f and ϕ_f are the magnitude and the phase of the forcing frequency (S_f) term, and $A_{1/3}$ and $\phi_{1/3}$ are those of the shedding frequency ($\frac{1}{3}S_f$) term, respectively. Note that other frequency terms, except the dominant two frequencies (S_f and $\frac{1}{3}S_f$), are negligible in tertiary lock-on.

To discriminate the lock-on and to show the behaviour of each frequency component pertinent to the forcing phase information ($\theta = 2\pi S_f t$), a phase diagram is constructed (Baek & Sung 2000). The phase diagram of C_L is described by dividing $C_L(\theta)$ into two components, where the a-axis and b-axis are defined as $a(\theta) = C_L(\theta)\cos\theta$ and $b(\theta) = C_L(\theta)\sin\theta$, respectively. This indicates that the distance from the origin ($a = 0$, $b = 0$) is $C_L(\theta)$ and the angle with the a-axis is θ, i.e. $\tan\theta = b(\theta)/a(\theta)$. In figure 3, four phase diagrams for $S_f = 0.504$ are displayed, where the solid circle (a_f, b_f) and the dotted trajectory ($a_{1/3}$, $b_{1/3}$) represent the S_f term and the $\frac{1}{3}S_f$ ($= St_0^*$) term, respectively. The dash–dot line (a, b) is the sum of these two terms. These terms

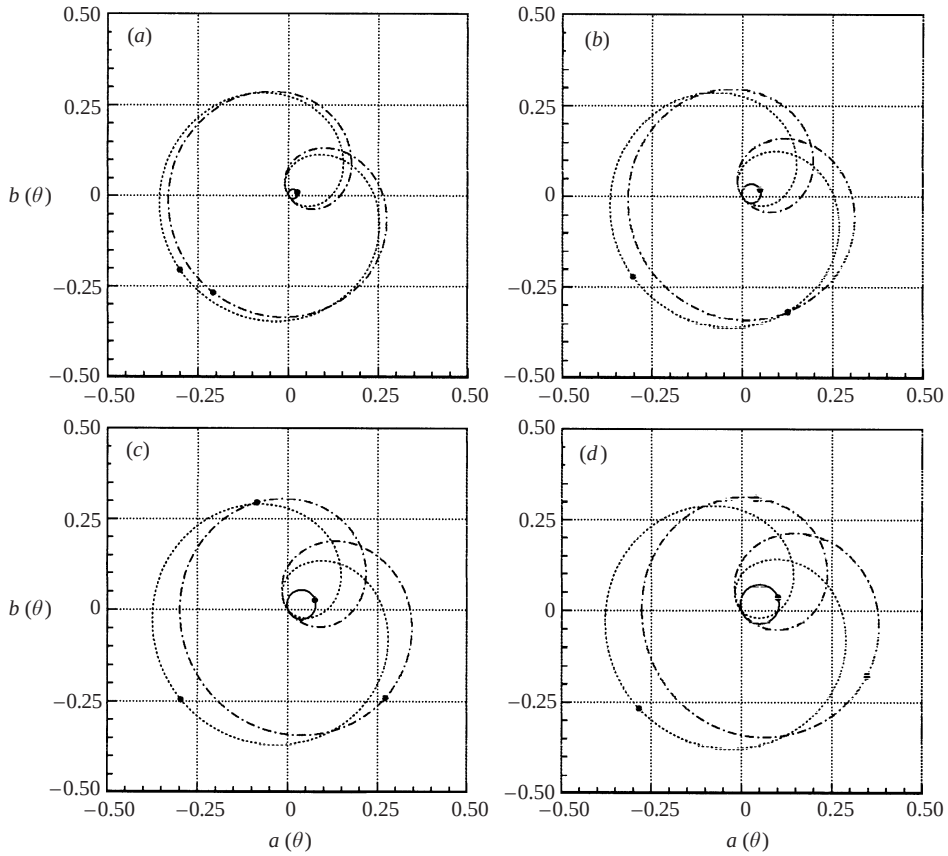

FIGURE 3. Phase diagrams of $C_L(\theta)$ for the tertiary superharmonic excitation ($S_f = 3St_0^* = 0.504$). ——, S_f; $\cdots$, $\frac{1}{3}S_f$; $- \cdot -$, sum. (*a*) $\Omega_{max} = 0.10$; (*b*) 0.20; (*c*) 0.30; (*d*) 0.40.

can be expressed as

$$a_f(\theta) = A_f \cos(2\pi S_f t - \phi_f)\cos\theta = A_f \cos(\theta - \phi_f)\cos\theta, \tag{3.2}$$

$$b_f(\theta) = A_f \cos(2\pi S_f t - \phi_f)\sin\theta = A_f \cos(\theta - \phi_f)\sin\theta, \tag{3.3}$$

$$a_{1/3}(\theta) = A_{1/3} \cos(2\pi \tfrac{1}{3} S_f t - \tfrac{1}{3}\phi_{1/3})\cos\theta = A_{1/3} \cos(\tfrac{1}{3}\theta - \tfrac{1}{3}\phi_{1/3})\cos\theta, \tag{3.4}$$

$$b_{1/3}(\theta) = A_{1/3} \cos(2\pi \tfrac{1}{3} S_f t - \tfrac{1}{3}\phi_{1/3})\sin\theta = A_{1/3} \cos(\tfrac{1}{3}\theta - \tfrac{1}{3}\phi_{1/3})\sin\theta, \tag{3.5}$$

$$a(\theta) = a_f(\theta) + a_{1/3}(\theta), \tag{3.6}$$

$$b(\theta) = b_f(\theta) + b_{1/3}(\theta). \tag{3.7}$$

Since the trajectories (a_f, b_f), ($a_{1/3}$, $b_{1/3}$) and (a, b) are a function of θ, the desired information for each component of $C_L(\theta)$ is acquired directly at each forcing phase θ. The maximum values are designated by black dots in figure 3. Based on the relations in equations (3.2)–(3.7), the dash–dot line (a, b) represents the instantaneous value of $C_L(t)$ at θ. The average value of the $\frac{1}{3}S_f$ term in equation (3.1) over three forcing periods is zero,

$$A_{1/3}\cos(\tfrac{1}{3}\theta - \tfrac{1}{3}\phi_{1/3}) + A_{1/3}\cos(\tfrac{1}{3}(\theta+2\pi) - \tfrac{1}{3}\phi_{1/3}) + A_{1/3}\cos(\tfrac{1}{3}(\theta+4\pi) - \tfrac{1}{3}\phi_{1/3}) = 0. \tag{3.8}$$

Accordingly, the solid circle (a_f, b_f) represents the average value of $C_L(t)$ at θ. For

the trajectory (a_f, b_f), a circle equation can be derived as

$$(a_f - \tfrac{1}{2}A_f \cos\phi_f)^2 + (b_f - \tfrac{1}{2}A_f \sin\phi_f)^2 = (\tfrac{1}{2}A_f)^2. \tag{3.9}$$

In the above circle equation, the distance from the origin ($a = 0$, $b = 0$) to the centre of circle ($\frac{1}{2}A_f \cos\phi_f$, $\frac{1}{2}A_f \sin\phi_f$) is $\frac{1}{2}A_f$. As seen in figure 3, the diagram of $(a_{1/3}, b_{1/3})$ depicts a heart-shape, not a circle. In the case of lock-on, since ϕ_f and $\phi_{1/3}$ are locked, the phase diagrams of S_f and $\frac{1}{3}S_f$ are closed, i.e. the value returns to the original one. If not locked, however, the trajectory (a, b) is not closed, but variant from cycle to cycle.

As in figure 3, $A_{1/3}$ is larger than A_f. This means that the most dominant frequency is $\frac{1}{3}S_f$ $(= St_0^*)$. A closer inspection of the solid circles (a_f, b_f) in figure 3 indicates that A_f increases with increasing Ω_{max}. However, the size of the diagram $(a_{1/3}, b_{1/3})$, i.e. $A_{1/3}$, remains nearly constant. This shows that the strength of the shedding vortex is not increased significantly. The $\frac{1}{3}S_f$ and S_f terms have one and three peaks over one vortex shedding cycle, respectively, i.e. $C_L(\theta)$ in equation (3.1) has one maximum for $A_f = 0$ and three for $A_{1/3} = 0$. As A_f increases, the aforestated combination of A_f and $A_{1/3}$ gives two maximum peaks in figure 2(c, d) at $\Omega_{max} \geqslant 0.30$. Since the maximum phases $(\phi_{1/3})$ of the $\frac{1}{3}S_f$ term are approximately out of phase with those (ϕ_f) of the S_f term, $C_L(\theta = \phi_{1/3})$ is smaller than $A_{1/3}$ in equation (3.1). In figure 3, ϕ_f and $\phi_{1/3}$ do not vary significantly. For $\Omega_{max} = 0.30$, the values of ϕ_f and $\phi_{1/3}$ are $\phi_f = 0.11\pi$ and $\phi_{1/3} = 1.22\pi$, respectively. The phases of the positive maximum are 0.59π and 1.77π. It is recalled that the rotational oscillation is defined as $\Omega = \Omega_{max} \sin(2\pi S_f t)$. The counterclockwise rotation occurs in the time 0 to $0.5T(\theta = \pi)$, and the clockwise rotation from $0.5T$ to $T(\theta = 2\pi)$. The positive maxima of instantaneous C_L occur when the clockwise and counterclockwise rotation velocities decrease. However, the positive maximum phase of average C_L is obtained when the counterclockwise rotation velocity increases. The phases of the negative maximum are opposite to those of the positive maximum.

Next, the forcing frequencies in the vicinity of $3St_0^* = 0.504$ are considered in figure 4. An examination of the lock-on range indicated that the tertiary lock-on occurs in the range $0.502 \leqslant S_f \leqslant 0.506$ at $\Omega_{max} = 0.10$ and $0.500 \leqslant S_f \leqslant 0.508$ at $\Omega_{max} = 0.30$. The increment of S_f for the lock-on test was 0.002. As Ω_{max} increases, the tertiary lock-on range widens. This is similar to the case of the primary lock-on. The time histories of C_L in the tertiary lock-on are displayed in figure 4. If the forcing magnitude is large $(\Omega_{max} = 0.30)$, two local maximum peaks are observed as in the case of $S_f = 0.504$ (figure 4c, d). Note that the vortex shedding frequency (St_0) is $\frac{1}{3}S_f$, not St_0^*. As mentioned earlier, the other frequency components are negligible.

In a manner similar to the derivation of equation (3.1), the values of A_f, $A_{1/3}$, ϕ_f and $\phi_{1/3}$ are determined by the imposed forcing magnitude and frequency. In the lock-on range, they are invariant from cycle to cycle. The corresponding phase diagrams are plotted in figure 5, where the same definitions of equations (3.2)–(3.7) are employed. A detailed comparison of the trajectories $(a_{1/3}, b_{1/3})$ for several forcing frequencies ($0.502 \leqslant S_f \leqslant 0.506$ for $\Omega_{max} = 0.10$ and $0.500 \leqslant S_f \leqslant 0.508$ for $\Omega_{max} = 0.30$) indicates that $\phi_{1/3}$ changes significantly over a small change of S_f. For example, as summarized in tables 1 and 2, $\phi_{1/3} = 1.02\pi$ at $S_f = 0.502$, and $\phi_{1/3} = 1.34\pi$ at $S_f = 0.506$ for $\Omega_{max} = 0.10$. For $\Omega_{max} = 0.30$, $\phi_{1/3} = 1.12\pi$ at $S_f = 0.500$, and $\phi_{1/3} = 1.34\pi$ at $S_f = 0.508$. This significant change of $\phi_{1/3}$ reflects the phase change of vortex shedding relative to the cylinder motion, which is similar to that of the primary lock-on. It is known that the phase shift in the primary lock-on is of the order of π.

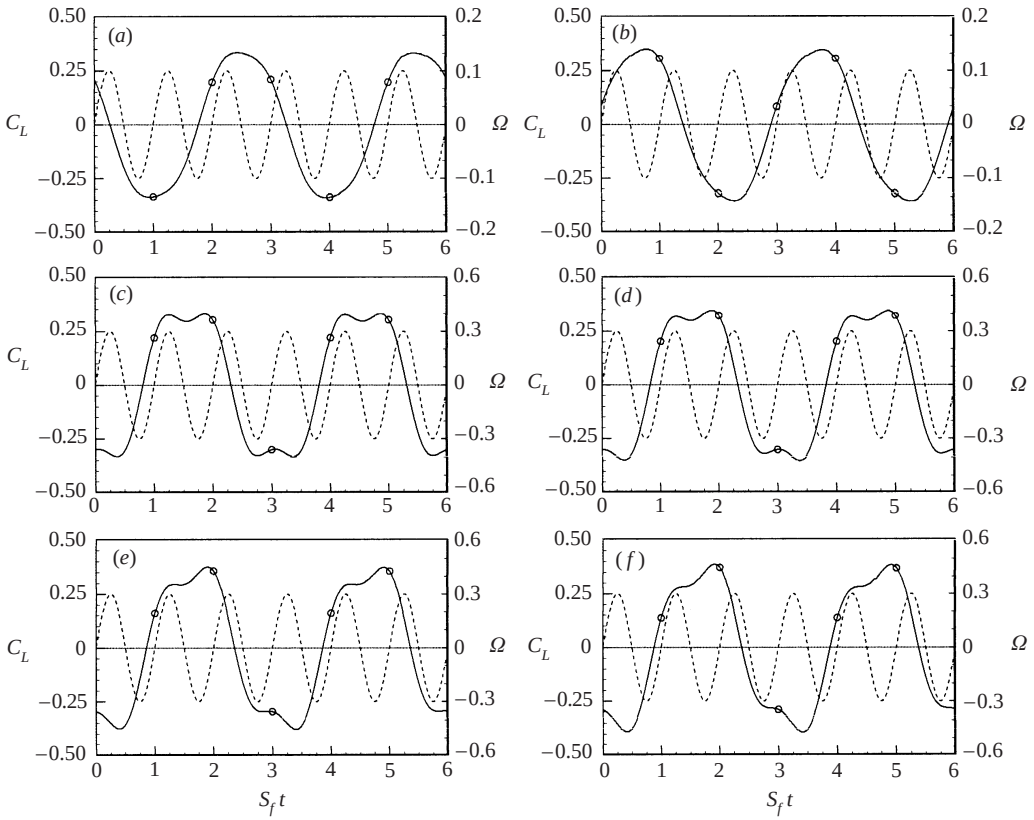

FIGURE 4. Time histories of $C_L(\theta)$ for the tertiary superharmonic excitation ($S_f \approx 3St_0^* = 0.504$). (*a*) $S_f = 0.502$, $\Omega_{max} = 0.10$; (*b*) 0.506, 0.10; (*c*) 0.500, 0.30; (*d*) 0.502, 0.30; (*e*) 0.506, 0.30; (*f*) 0.508, 0.30.

	$S_f = 0.502$	$S_f = 0.504$	$S_f = 0.506$
$\phi_{1/3}$	1.02π	1.19π	1.34π
ϕ_f	0.11π	0.11π	0.11π

TABLE 1. The phase angles at $\Omega_{max} = 0.10$.

	$S_f = 0.500$	$S_f = 0.502$	$S_f = 0.504$	$S_f = 0.506$	$S_f = 0.508$
$\phi_{1/3}$	1.12π	1.17π	1.22π	1.28π	1.34π
ϕ_f	0.11π	0.11π	0.11π	0.11π	0.11π

TABLE 2. The phase angles at $\Omega_{max} = 0.30$.

However, the phase shift in the tertiary lock-on is smaller than π. The phase shift rate of $\phi_{1/3}$ at $\Omega_{max} = 0.10$ is larger than that at $\Omega_{max} = 0.30$, because the lock-on range at $\Omega_{max} = 0.10$ is smaller than that at $\Omega_{max} = 0.30$. On the contrary, the maximum phase (ϕ_f) of average C_L remains nearly constant, i.e. $\phi_f = 0.11\pi$ at $S_f = 0.500$, and $\phi_f = 0.11\pi$ at $S_f = 0.508$ for $\Omega_{max} = 0.30$.

It is important to look into the vortex shedding pattern with respect to the rotational oscillation in the tertiary lock-on. To observe the vortex formation mode,

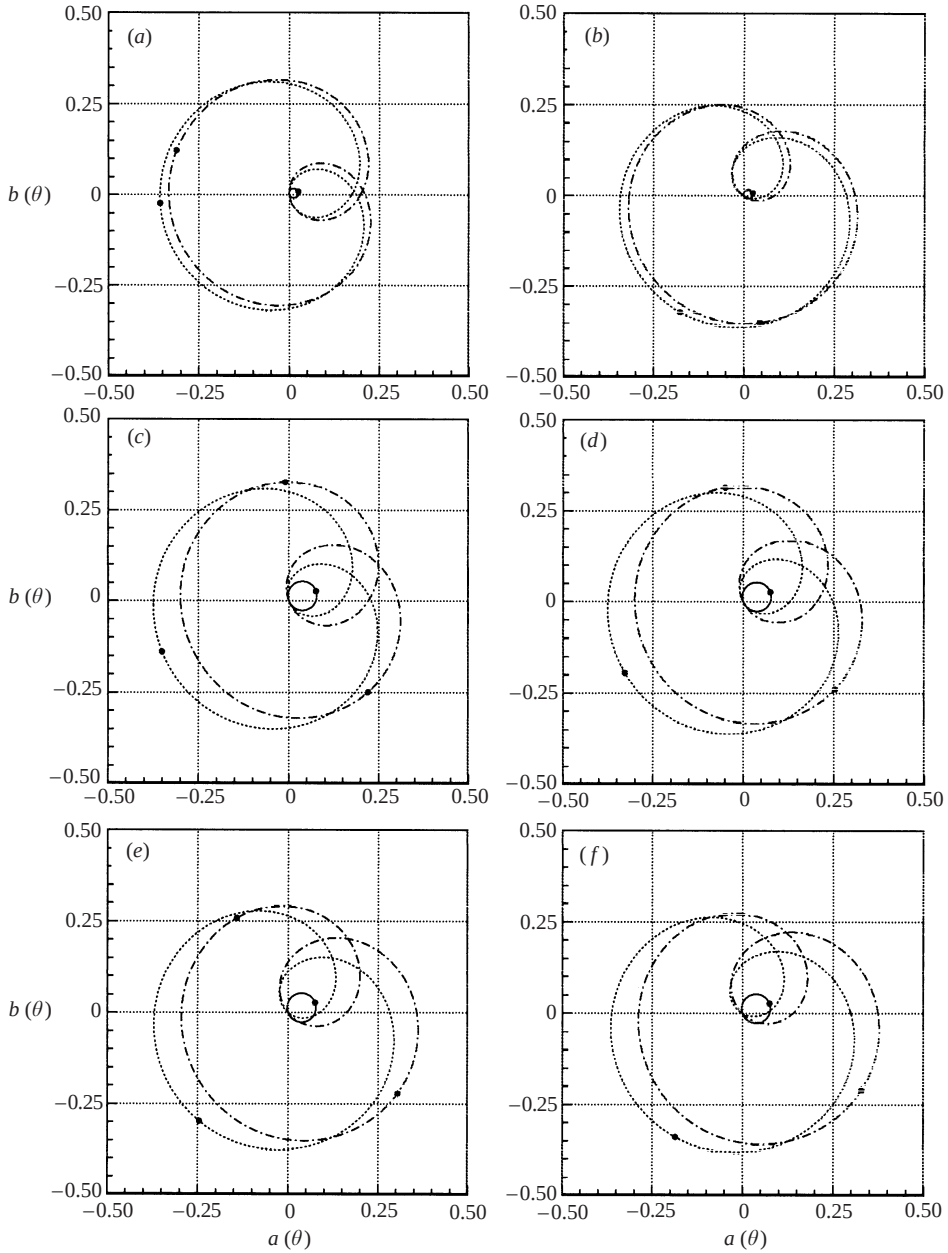

FIGURE 5. Phase diagrams of $C_L(\theta)$ for the tertiary superharmonic excitation ($S_f \approx 3St_0^* = 0.504$): ——, S_f; ···, $\frac{1}{3}S_f$; — · —, sum. (*a*) $S_f = 0.502$, $\Omega_{max} = 0.10$; (*b*) 0.506, 0.10; (*c*) 0.500, 0.30; (*d*) 0.502, 0.30; (*e*) 0.506, 0.30; (*f*) 0.508, 0.30.

the vorticity contours are displayed in figure 6 at $S_f = 0.504$ and $\Omega_{max} = 0.30$. The snapshots are taken with the interval $\Delta\theta = \frac{1}{4}\pi$ over the $\frac{3}{2}$ forcing cycles. The $\frac{3}{2}$ forcing cycles correspond to a half of the vortex shedding cycle. The time history of $C_L(\theta)$ is also plotted on the upper left-hand side of the figure. The designated points in $C_L(\theta)$ correspond to the respective instants in the vorticity contours. In the present study, the vorticity distributions are adopted instead of the streamline patterns. In

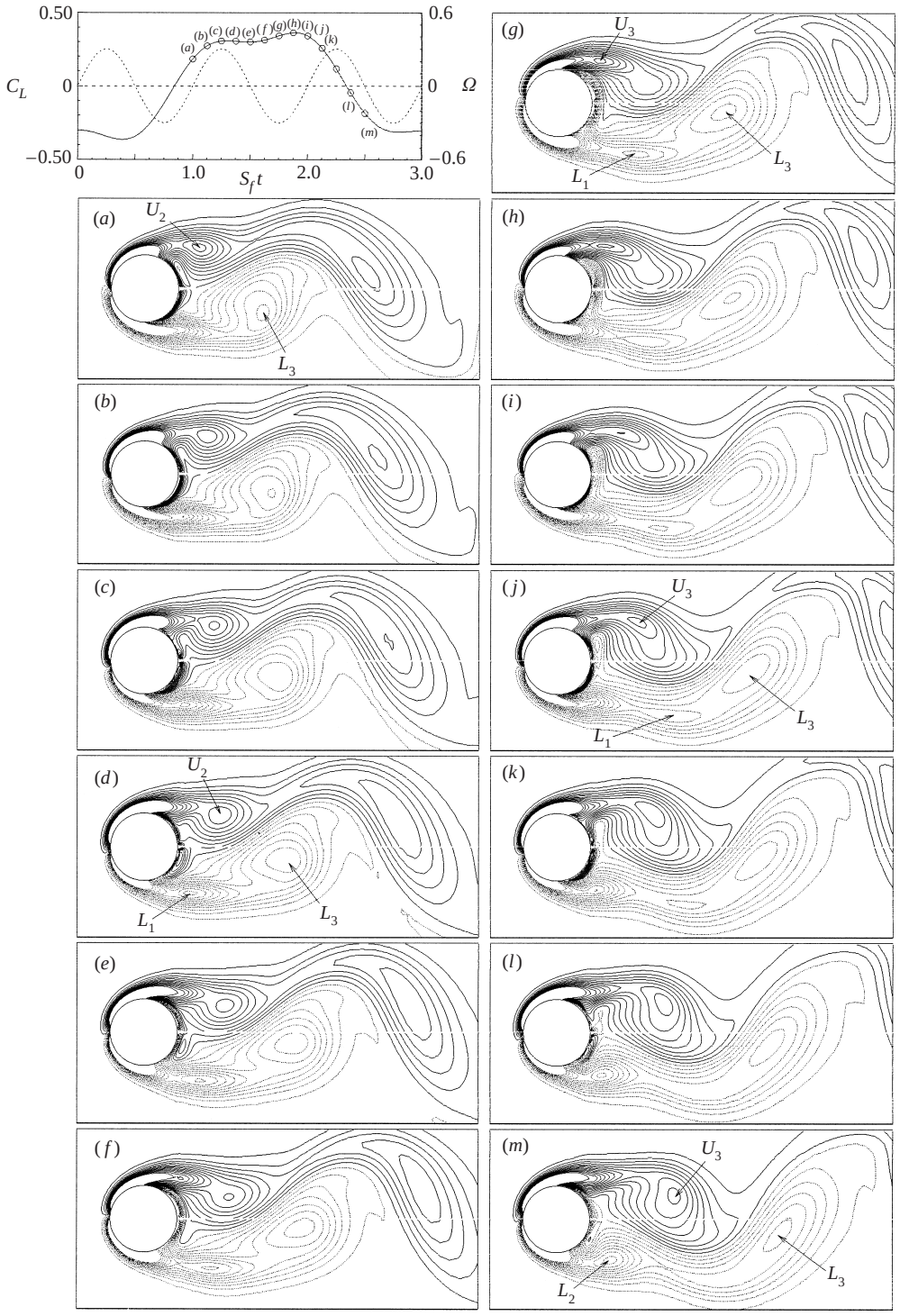

FIGURE 6. Vorticity contours at $S_f = 0.504$ and $\Omega_{max} = 0.30$. The points in the $C_L(t)$ diagram correspond to the respective instants in the vorticity contours.

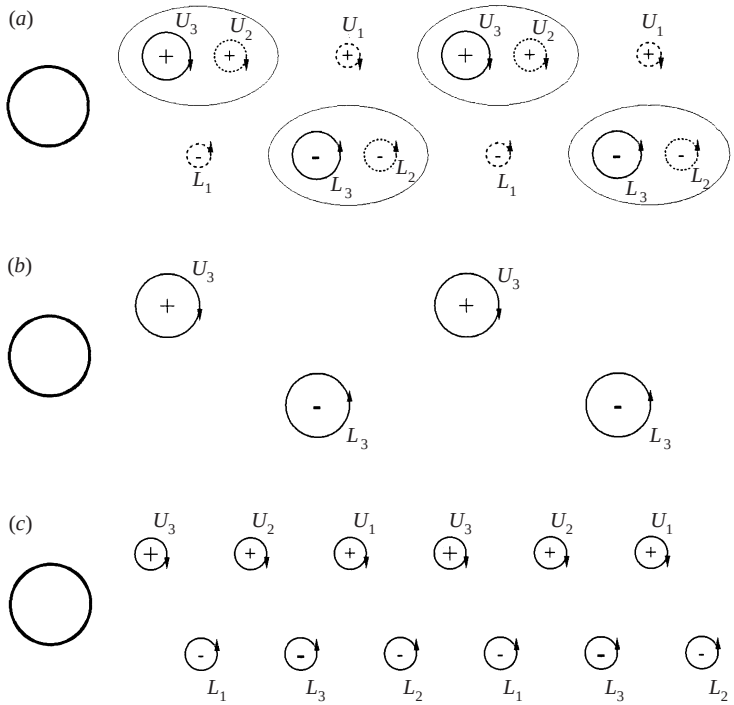

FIGURE 7. Schematic diagram of the vortex formation patterns for the tertiary superharmonic excitation. (*a*) Tertiary lock-on. (*b*) Natural shedding. (*c*) Primary lock-on.

the streamline patterns, larger-scale vortices are clearly displayed. However, smaller circulations are not captured by the streamlines (Lin & Rockwell 1997). Furthermore, a single reference frame of the streamline cannot properly represent the entire vortex system in the immediate vicinity of the cylinder surface. It is known that the vorticity layers are separated from the shoulders of the cylinder and the separation point moves to the base of the cylinder at sufficiently large amplitude (Sheridan *et al.* 1998).

In figure 6, three vortices are formed from each shoulder of the cylinder over three forcing periods. Only one vortex among them is convected in the far downstream. For convenience, the vortices in the upper side are termed U_1, U_2 and U_3 in sequence. These are generated in the clockwise sense. Similarly, the vortices in the lower side with the counterclockwise sense are L_1, L_2 and L_3. Once one vortex is created, a low-pressure region emerges to balance its centrifugal force. The cylinder is then forced to the direction where the vortex evolves. It is seen that U_2 and U_3 are formed at (*a*)–(*c*) and (*g*)–(*i*) in figure 6. At this instance, C_L is positive. However, L_1 is formed in the lower side at (*d*)–(*f*) between the formations of U_2 and U_3. It is seen that C_L is not monotonically increased. After a small decrease by L_1, C_L increases and then becomes maximum, i.e. two local maximum peaks are visible. Although three vortices are generated from each side, only one vortex (U_3) is convected in the downstream from each side. As time goes by, L_1 disappears and U_2 merges with U_3. Note that figure 6(*m*) is a mirror image of figure 6(*a*), in which L_2 is formed at (*m*) like U_2 at (*a*). These patterns are repeated in the upper and lower regions of the wake in a π out-of-phase fashion.

To gain a better understanding, a schematic diagram of the vortex formation patterns in figure 6 is plotted in figure 7(*a*). This gives an overview of the characteristics of vortex formation and shedding for the tertiary lock-on. The vortex strengths are

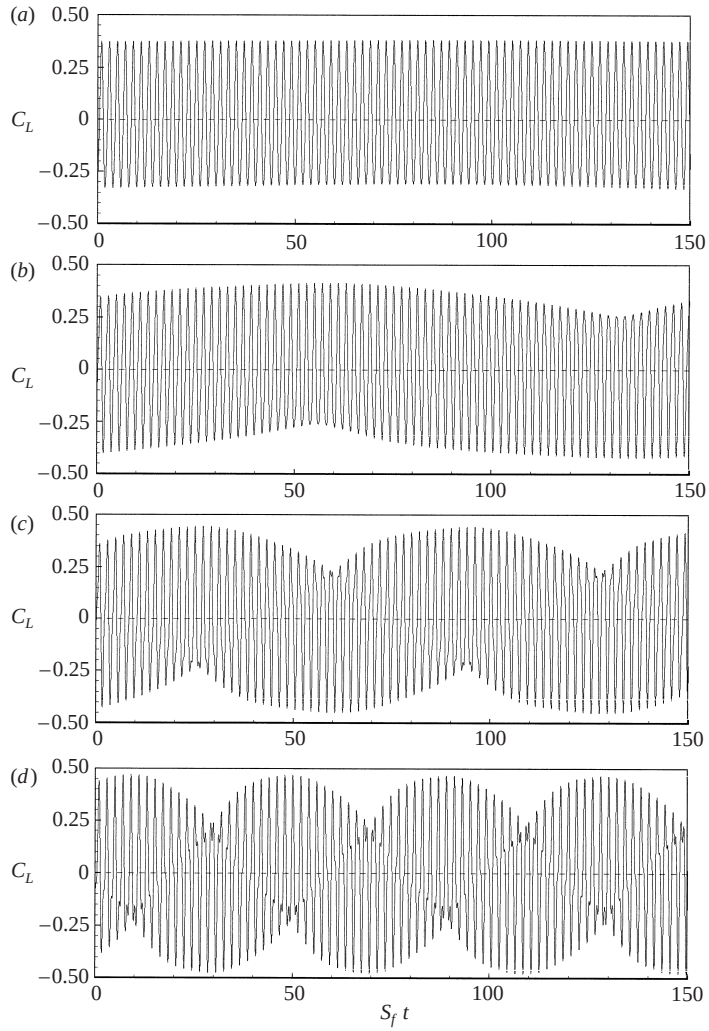

FIGURE 8. Time histories of $C_L(\theta)$ for the secondary superharmonic excitation ($S_f = 2St_0^* = 0.336$). (*a*) $\Omega_{max} = 0.10$; (*b*) 0.20; (*c*) 0.30; (*d*) 0.40.

$U_1 < U_2 < U_3$ and $L_1 < L_2 < L_3$, respectively. Recall that C_L is positive when U_2 and U_3 are formed and negative when L_2 and L_3 are formed. The small decrease of C_L in the inset of figure 6 is caused by U_1 and L_1. If the forcing magnitude is zero ($\Omega_{max} = 0$), the S_f component is zero and only St_0^* exists. Since the strengths of U_1, U_2, L_1 and L_2 are zero, the vortex shedding with only U_3 and L_3 is observed in figure 7(*b*). However, when the forcing magnitude is sufficiently large, the tertiary lock-on returns to the primary lock-on. The vortex strengths are then equivalent, $U_1 = U_2 = U_3$, $L_1 = L_2 = L_3$. Only the S_f component exists, where the vortex pattern is displayed in figure 7(*c*). Figure 7(*a*) is an intermediate pattern of figures 7(*b*) and 7(*c*) with different vortex strengths, which belongs to the tertiary lock-on.

4. Response to the secondary superharmonic excitation

As remarked earlier, the main purpose of the present study is to identify the existence of the secondary lock-on. Toward this end, the forcing frequency is set to

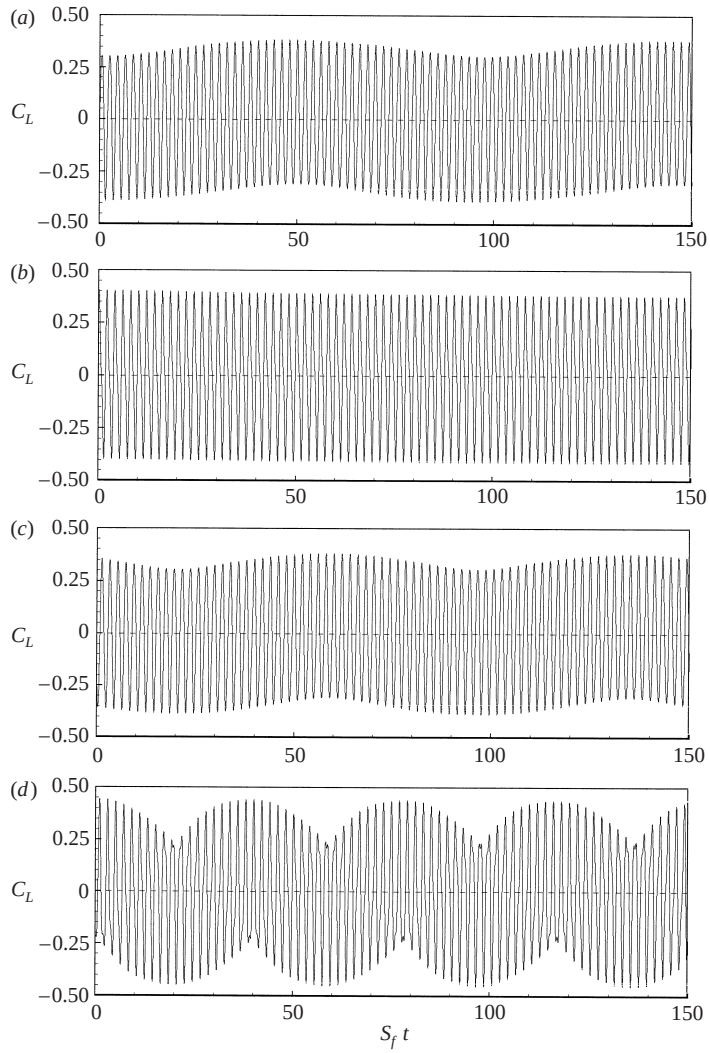

FIGURE 9. Time histories of $C_L(\theta)$ for the secondary superharmonic excitation ($S_f \approx 2St_0^* = 0.336$). (*a*) $S_f = 0.332$, $\Omega_{max} = 0.10$; (*b*) 0.332, 0.30; (*c*) 0.340, 0.10; (*d*) 0.340, 0.30.

be about two times the natural shedding frequency (St_0^*=0.168), i.e. $S_f = 0.336$. Four forcing amplitudes are applied, $\Omega_{max} = 0.10$, 0.20, 0.30 and 0.40. Time histories of C_L are displayed in figure 8 at $S_f = 0.336$. As can be seen, the lock-on does not occur, but modulated oscillations are observed. As Ω_{max} increases at a fixed S_f, the modulated period decreases. On the surface, the time history of C_L at $\Omega_{max} = 0.10$ in figure 8(*a*) is seen to be locked-on. However, it is not really locked-on, but has a very long modulated period. To examine the long modulated period pertinent to the forcing conditions, the forcing frequencies in the vicinity of $2St_0^*$ are imposed, i.e. $S_f = 0.332$ and $S_f = 0.340$ (figure 9). These are slightly below and above $2St_0^*$. In these cases, modulated oscillations are clearly observed. A closer inspection of the time history of C_L in figure 9(*a*) reveals that the modulated period at $S_f = 0.332$ and $\Omega_{max} = 0.10$ is shorter than that at $S_f = 0.336$ and $\Omega_{max} = 0.10$. However, the modulated period at $S_f = 0.332$ and $\Omega_{max} = 0.30$ is much longer than that at

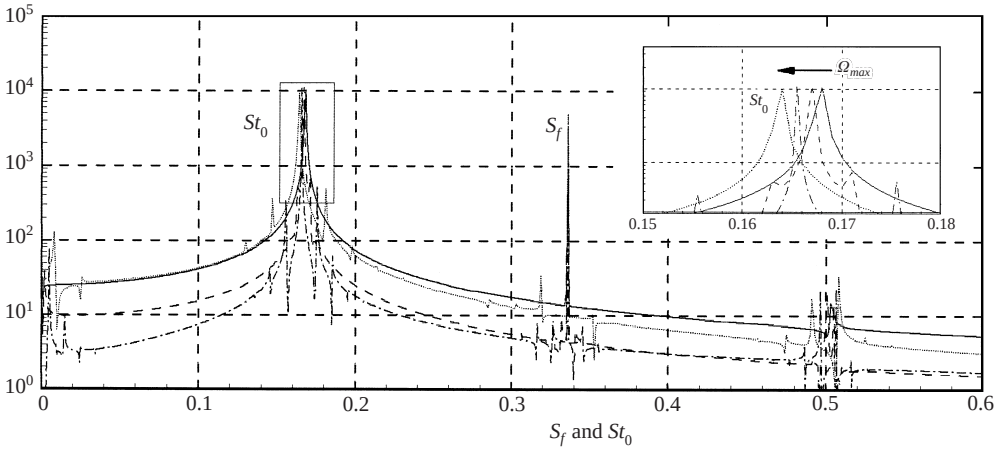

FIGURE 10. Power spectra at $S_f = 0.336$ for $\Omega_{max} = 0.10$, 0.20, 0.30 and 0.40.

$S_f = 0.336$ and $\Omega_{max} = 0.30$. The time history of C_L at $S_f = 0.332$ and $\Omega_{max} = 0.30$ has a very long period, which is similar to the case at $S_f = 0.336$ and $\Omega_{max} = 0.10$. For $S_f = 0.340$, as Ω_{max} increases, the modulated period decreases. Moreover, the modulated period at $S_f = 0.340$ and $\Omega_{max} = 0.30$ in figure 9(d) is shorter than that at $S_f = 0.336$ and $\Omega_{max} = 0.30$ in figure 8(c). This suggests that the secondary lock-on does not exist due to the modulated oscillations.

In order to analyse the modulated oscillations in detail, the time histories of C_L at $S_f = 0.336$ in figure 8 are Fourier-transformed and the results are displayed in figure 10. The forcing frequency is clearly detected at $S_f = 0.336$. An inspection of the shedding frequencies (St_0) subjected to several forcing amplitudes discloses that they are not concentrated at half of the forcing frequency, i.e. $\frac{1}{2}S_f$ ($= St_0^*$). The inset indicates that, as Ω_{max} increases, St_0 gradually moves from St_0^* to lower values. It is important to find these shift phenomena in a sense that St_0 is not half of S_f ($St_0 \neq \frac{1}{2}S_f$). This slight discrepancy reproduces the aforestated modulated oscillations, i.e. the secondary lock-on does not exist. The modulated oscillation frequency is defined as $\frac{1}{2}S_f - St_0$. As the discrepancy increases, the modulated oscillation period decreases. Note that the present gradual shift of St_0 is consistent with the experimental results (Stansby 1976; Ongoren & Rockwell 1988; Willams, Mansy & Amato 1992). Here, the forcing frequency of the secondary lock-on is lower than $2St_0^*$. In the primary lock-on region, the forcing frequency of the sudden phase shift decreases with increasing forcing magnitude (Stansby 1976). It is seen that St_0 is dominant in magnitude among the other respective frequencies. The power spectra in figure 10 show that small distorted frequency components exist due to the nonlinear coupling effect.

The time history of C_L of the secondary superharmonic excitation can be described in terms of S_f and $\frac{1}{2}S_f$, which is similar to the tertiary superharmonic excitation in equation (3.1),

$$\begin{aligned} C_L(t) &= A_f \cos(2\pi S_f t - \phi_f) + A_{1/2} \cos(2\pi \tfrac{1}{2} S_f t - \tfrac{1}{2}\phi_{1/2}) \\ &= A_f \cos(\theta - \phi_f) + A_{1/2} \cos(\tfrac{1}{2}\theta - \tfrac{1}{2}\phi_{1/2}). \end{aligned} \tag{4.1}$$

Here, A_f and ϕ_f are the magnitude and phase of S_f, and $A_{1/2}$ and $\phi_{1/2}$ are those of $\frac{1}{2}S_f$, respectively. These values of A_f, $A_{1/2}$, ϕ_f and $\phi_{1/2}$ are determined by S_f and Ω_{max}.

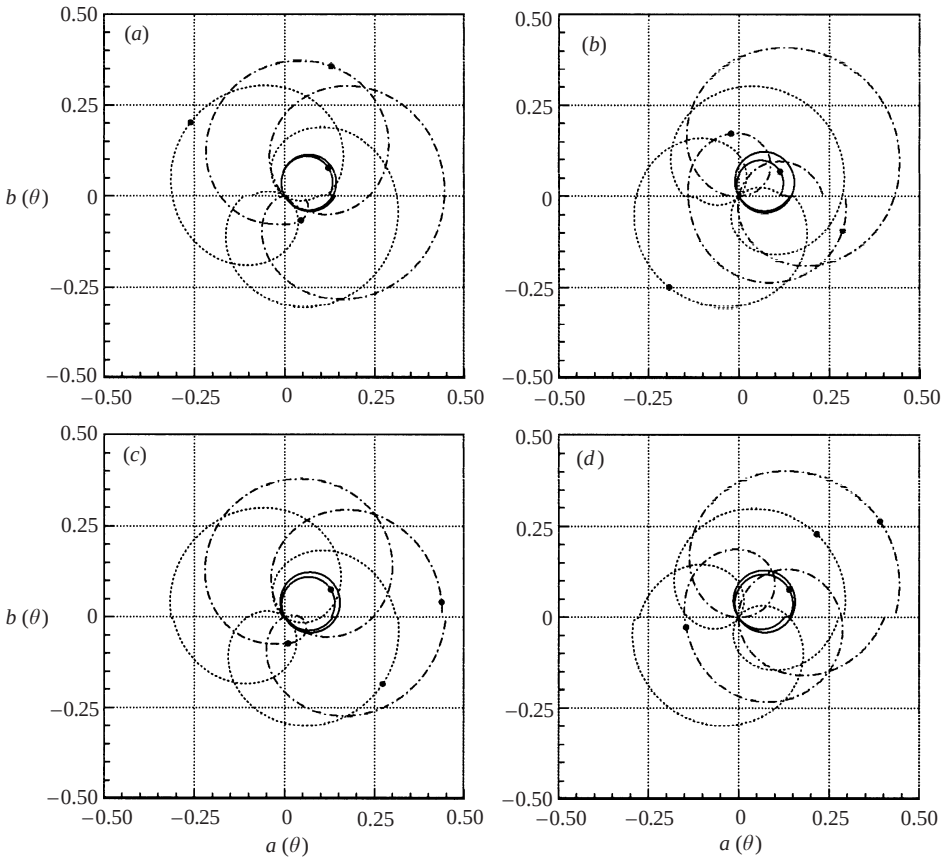

FIGURE 11. Phase diagrams of $C_L(\theta)$ for $S_f = 0.336$ and $\Omega_{max} = 0.40$. ——, S_f; $\cdots$, $\frac{1}{2}S_f$; $- \cdot -$, sum. (*a*) $S_f t = 100 \sim 102$; (*b*) $110 \sim 112$; (*c*) $120 \sim 122$; (*d*) $140 \sim 142$.

In the case of lock-on, these are invariant. However, they are variant in the present case of non-lock-on.

The phase diagrams of C_L are displayed in a manner similar to the tertiary superharmonic excitation in figure 11. Four time sets for two forcing periods at $S_f = 0.336$ and $\Omega_{max} = 0.40$ are selected in figure 11. Contrary to the tertiary lock-on, the diagrams are variant from cycle to cycle by the modulated oscillations. The solid trajectory (a_f, b_f) denotes the average value over two forcing cycles,

$$a_f(\theta) = \tfrac{1}{2}\{C_L(\theta) + C_L(\theta + 2\pi)\}\cos\theta \approx A_f \cos(\theta - \phi_f)\cos\theta, \tag{4.2}$$

$$b_f(\theta) = \tfrac{1}{2}\{C_L(\theta) + C_L(\theta + 2\pi)\}\sin\theta \approx A_f \cos(\theta - \phi_f)\sin\theta. \tag{4.3}$$

If $A_{1/2}$ and $\phi_{1/2}$ in equation (4.1) are time-invariant owing to lock-on, the average of the $\frac{1}{2}S_f$ term in equation (4.1) over two forcing periods is zero,

$$A_{1/2}\cos(\tfrac{1}{2}\theta - \tfrac{1}{2}\phi_{1/2}) + A_{1/2}\cos(\tfrac{1}{2}(\theta + 2\pi) - \tfrac{1}{2}\phi_{1/2}) = 0. \tag{4.4}$$

However, since it is not locked-on, the shape of (a_f, b_f) is not a closed circle. The dash–dot line (a, b) denotes the instantaneous C_L and the dotted line $(a_{1/2}, b_{1/2})$

represents the difference between (a_f, b_f) and (a, b).

$$a(\theta) = C_L(t)\cos(\theta), \tag{4.5}$$

$$b(\theta) = C_L(t)\sin(\theta), \tag{4.6}$$

$$a_{1/2}(\theta) = a(\theta) - a_f(\theta) \approx A_{1/2}\cos(\tfrac{1}{2}\theta - \tfrac{1}{2}\phi_{1/2})\cos\theta, \tag{4.7}$$

$$b_{1/2}(\theta) = b(\theta) - b_f(\theta) \approx A_{1/2}\cos(\tfrac{1}{2}\theta - \tfrac{1}{2}\phi_{1/2})\sin\theta. \tag{4.8}$$

Owing to the modulated oscillations, C_L does not return to the original value after two forcing periods, i.e. $C_L(\theta) \neq C_L(\theta + 4\pi)$. Accordingly, these trajectories are not closed. The maximum points are designated by black dots in figure 11. The points on (a_f, b_f) indicate the values of A_f and ϕ_f. The values of $A_{1/2}$ and $\phi_{1/2}$ are expressed by the points on $(a_{1/2}, b_{1/2})$. It is seen in figure 11 that the variations of A_f, $A_{1/2}$ and ϕ_f are not substantial. However, the variation of $\phi_{1/2}$ is significant from cycle to cycle. It is assumed that the time variation of $\phi_{1/2}$ induces the aforestated modulated oscillations.

The shedding frequency St_0 in the power spectra of figure 10 can be defined by both $\frac{1}{2}S_f$ and the time change rate of $\phi_{1/2}$. An examination of figure 11 reveals that $\phi_{1/2}$ changes linearly,

$$\phi_{1/2} = 4\pi\Delta St\, t + \phi_{1/2_0}. \tag{4.9}$$

Here, $\phi_{1/2_0}$ denotes the initial value of $\phi_{1/2}$. The substitution of equation (4.9) into equation (4.1) gives

$$\begin{aligned} C_L(t) &= A_f\cos(2\pi S_f t - \phi_f) + A_{1/2}\cos(2\pi[\tfrac{1}{2}S_f t - \Delta St]t - \tfrac{1}{2}\phi_{1/2_0}) \\ &= \underbrace{A_f\cos(2\pi S_f t - \phi_f)}_{S_f \text{ term}} + \underbrace{A_{1/2}\cos(2\pi St_0 t - \tfrac{1}{2}\phi_{1/2_0})}_{St_0 \text{ term}}, \end{aligned} \tag{4.10}$$

where St_0 is defined as $\frac{1}{2}S_f - \Delta St$, which is close to St_0^*. It is seen in figure 10 that St_0 is gradually shifted to lower frequencies as Ω_{max} increases. In equation (4.10), A_f, ϕ_f, $A_{1/2}$, St_0 and $\phi_{1/2_0}$ are constant.

In the secondary superharmonic excitation, although only one frequency component is forced, the cylinder wake generates multiple fundamental frequency components. This state can be called 'quasi-periodicity', where the state has a period of infinity and does not close itself in the phase-plane. The Fourier transform of the periodic state consists of delta function spikes located at integer multiples of the fundamental frequency. The quasi-periodic state can be thought of as a mixture of periodic motions of several different fundamental frequencies. The Fourier transform of the quasi-periodic system consists of delta function spikes at all integer combinations of fundamental frequencies (figure 10). Since it contains only discrete components, it should be distinguished from a chaotic system that has a broad continuous component distribution (Ott 1993; Baek & Sung 2000).

Taking a phase-average at every θ $(= 2\pi S_f t)$, the St_0 term in equation (4.10) goes to zero. This is due to the fact that St_0/S_f is irrational, i.e. it exhibits quasi-periodicity. The average and the maximum of $C_L(\theta)$ are then written as,

$$C_{L_{ave}}(\theta) = A_f\cos(2\pi S_f t - \phi_f) = A_f\cos(\theta - \phi_f), \tag{4.11}$$

$$C_{L_{max}}(\theta) = A_f\cos(2\pi S_f t - \phi_f) + A_{1/2} = A_f\cos(\theta - \phi_f) + A_{1/2}. \tag{4.12}$$

The phase diagrams of $C_{L_{max}}(\theta)$ for $S_f = 2St_0^*$ are displayed in figure 12. The solid circle (a_f, b_f) and the dash-dot circle $(a_{1/2}, b_{1/2})$ represent the S_f term and the St_0

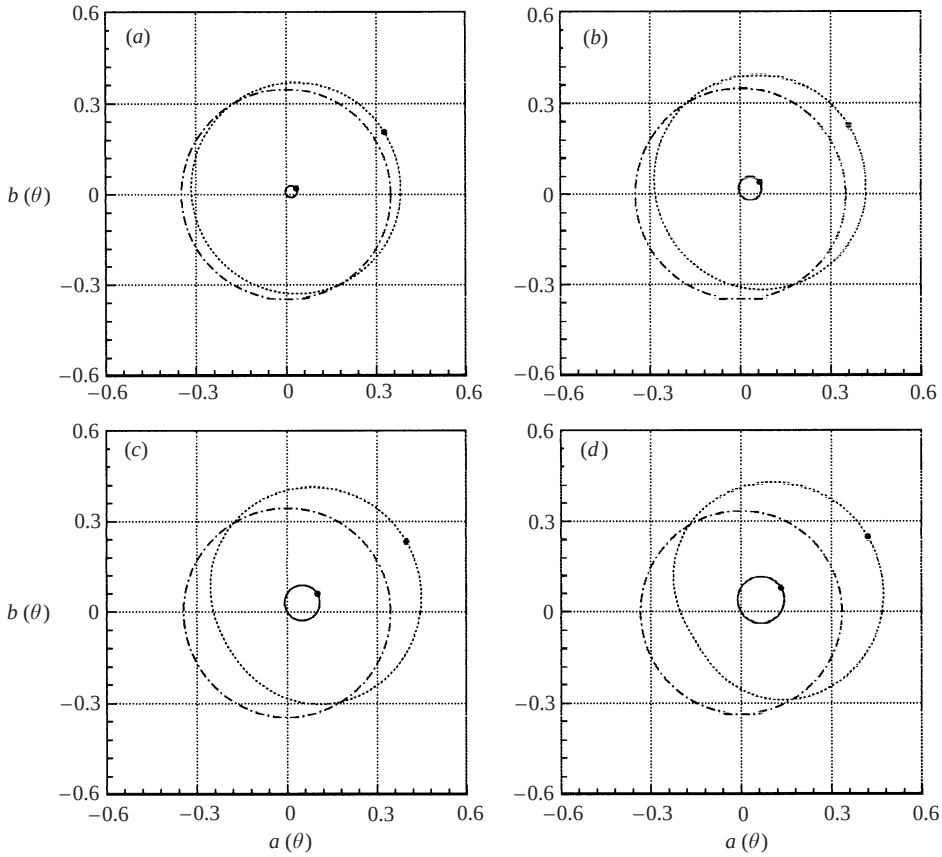

FIGURE 12. Phase diagrams of $C_{L_{max}}(\theta)$ for the secondary superharmonic excitation ($S_f = 2St_0^* = 0.336$). ——, S_f; — · —, St_0; · · ·, sum. (*a*) $\Omega_{max} = 0.10$; (*b*) 0.20; (*c*) 0.30; (*d*) 0.40.

term, respectively. The dotted line (a, b) is the sum of these two terms. They are defined as,

$$a_f(\theta) = A_f \cos(2\pi S_f t - \phi_f)\cos\theta = A_f \cos(\theta - \phi_f)\cos\theta, \tag{4.13}$$

$$b_f(\theta) = A_f \cos(2\pi S_f t - \phi_f)\sin\theta = A_f \cos(\theta - \phi_f)\sin\theta, \tag{4.14}$$

$$a_{1/2}(\theta) = A_{1/2}\cos\theta, \tag{4.15}$$

$$b_{1/2}(\theta) = A_{1/2}\sin\theta. \tag{4.16}$$

The phase diagram of $C_{L_{ave}}(\theta)$ is a circle of (a_f, b_f) itself. With these definitions, the behaviour of $C_L(t)$ versus θ can be analysed with respect to S_f. The marked points in the solid line indicate the maximum phases of $C_{L_{ave}}(\theta)$ and $C_{L_{max}}(\theta)$, respectively. The maximum phase of $C_{L_{max}}(\theta)$ is equal to that of $C_{L_{ave}}(\theta)$, e.g. $\theta_f = 0.17\pi$ at $\Omega_{max} = 0.30$. This suggests that the positive maximum of $C_{L_{ave}}(\theta)$ is obtained when the counterclockwise velocity increases. It is known from the definition of $C_{L_{max}}(\theta)$ that all instantaneous points of $a(t)$ and $b(t)$ are encompassed within the dash–dot trajectory (a, b). The dotted line (a, b) indicates the range of $C_L(t)$ at θ, e.g. $-0.245 \leqslant C_L(\theta = 0) \leqslant 0.445$ and $C_{L_{ave}}(\theta = 0) = 0.100$ at $\Omega_{max} = 0.30$. The size of (a_f, b_f) increases as Ω_{max} increases in figure 12, which is consistent with the case of the tertiary lock-on. The sizes of ($a_{1/2}$, $b_{1/2}$) are nearly constant. This means that the

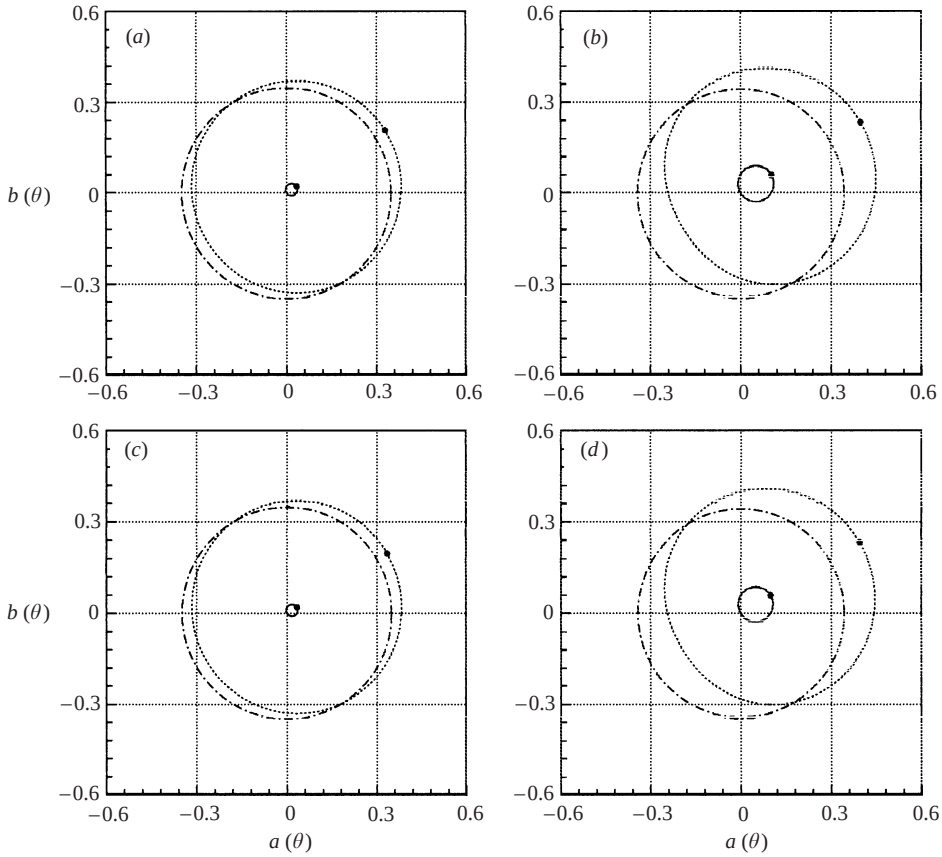

FIGURE 13. Phase diagrams of $C_{L_{max}}(\theta)$ for the secondary superharmonic excitation ($S_f \approx 2St_0^* = 0.336$). ——, S_f; — · —, St_0; ···, sum. (*a*) $S_f = 0.332$, $\Omega_{max} = 0.10$; (*b*) 0.332, 0.30; (*c*) 0.340, 0.10; (*d*) 0.340, 0.30.

strengths of shedding vortices are not significantly affected by Ω_{max} and S_f. Since the change of ϕ_f is not substantial, the maximum phase of average C_L is preserved. The phase diagrams of $C_{L_{max}}(\theta)$ at $S_f = 0.332$ and $S_f = 0.340$ are also shown in figure 13. The behaviours of A_f, $A_{1/2}$ and ϕ_f are similar to those of $S_f = 0.336$. The values of A_f, $A_{1/2}$ and ϕ_f remain nearly constant with respect to S_f. The influence of S_f is very weak except for the modulated period.

The vorticity contours are shown in figure 14 at $S_f = 0.336$ and $\Omega_{max} = 0.40$. Since the secondary lock-on does not occur, the vortex formation and shedding patterns are variant from cycle to cycle. The snapshots are taken with the interval $\Delta\theta = \frac{1}{2}\pi$ over two forcing periods. The designated points in $C_L(t)$ correspond to the respective instants in the vorticity contours. Two vortices from each side are formed over two forcing cycles, however, only one vortex is convected in the far downstream. U_1, U_2, L_1 and L_2 are termed in a manner similar to the case in figure 6. C_L increases when U_1 and U_2 are formed at figure 14(a, b) and figure 14(d, e). However, L_1 is formed in the opposite lower side at figure 14(b, c), which yields a small decrease in $C_L(t)$. When L_2 is formed and shed at figure 14(f, h), the values of C_L are negative. Although the vorticity contours at figure 14(a) are seen to be similar to those at figure 14(i), these are not exactly the same owing to the quasi-periodicity. Since St_0 is lower than half

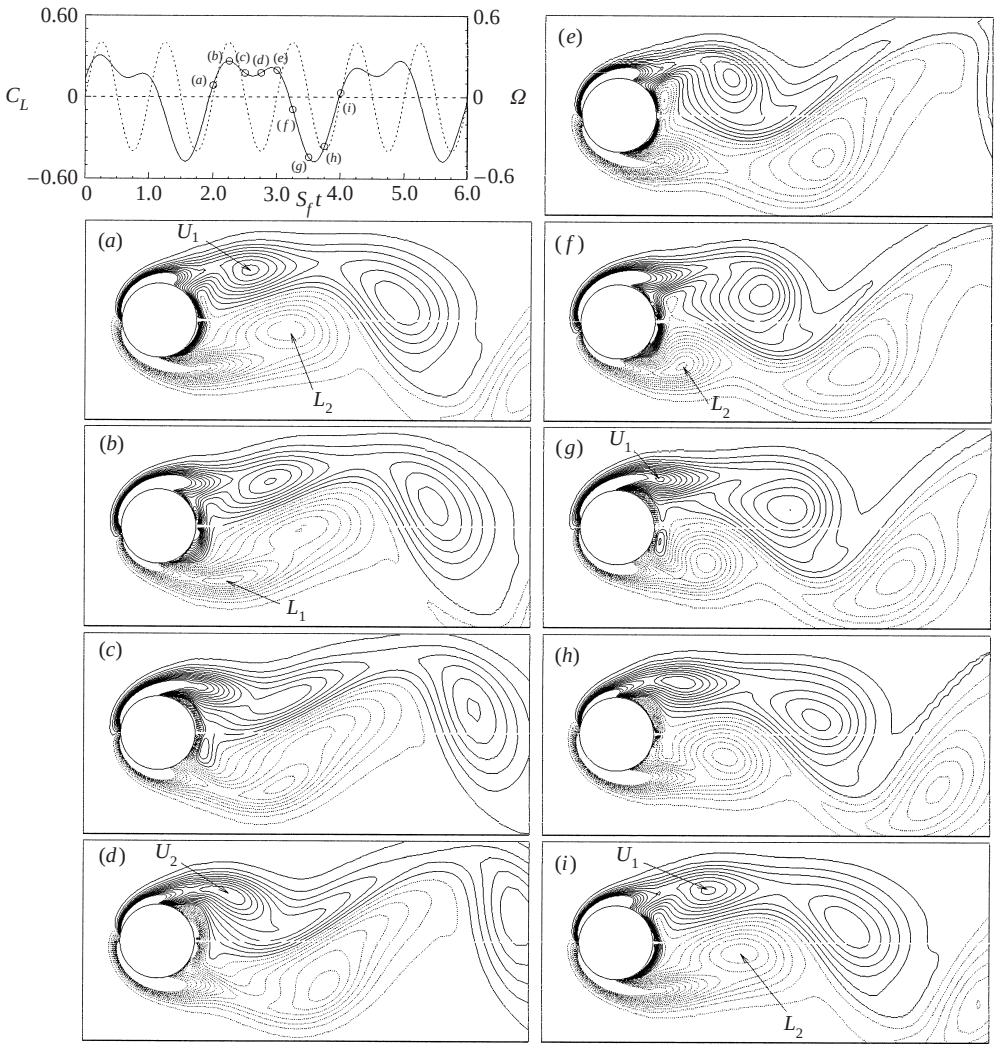

FIGURE 14. Vorticity contours at $S_f = 0.336$ and $\Omega_{max} = 0.40$. The points in the $C_L(t)$ diagram correspond to the respective instants in the vorticity contours.

of the forcing frequency ($S_f = 0.336$), the shedding period is longer than twice the forcing frequency. A small amount of additional time is required to return to the same value of C_L. Contrary to the tertiary lock-on, the vortex shedding pattern in the upper side is not the same as in the lower side. This is a manifestation of 'non-lock-on'.

The non-occurrence of the secondary lock-on can be elucidated by examining equations (3.1), (4.1) and (4.10). Since the present rotary oscillation is one of the antisymmetric forcings, a mirror image at the forcing phase θ should be reconstructed at the forcing phase $\theta + \pi$. In the lock-on state, the mirror image occurs after half of the vortex shedding period, as shown in figures 6(*a*) and 6(*m*). In the tertiary superharmonic excitation, after half of the vortex shedding period ($\theta + 3\pi$), the value of $C_L(\theta + 3\pi)$ in equation (3.1) is equal to that of $-C_L(\theta)$. This suggests that the lock-on exists in the tertiary excitation. On the contrary, in the secondary superharmonic excitation, the value of $C_L(\theta + 2\pi)$ in equation (4.1) is not equal to that of $-C_L(\theta)$,

where the lock-on does not exist. After a long time T, a mirror image can be obtained by the quasi-periodicity in equation (4.10), i.e. $T = (2n+1)/2S_f = (2m+1)/2St_0$. Here, n and m are integers. Since St_0/S_f is irrational, T is infinite. An exact mirror image is not obtainable, but it comes close to a mirror image. In the general nth superharmonic excitation, after half of the vortex shedding period ($\Delta\theta = n\pi$), $C_L(\theta + n\pi)$ can be expressed as

$$C_L(\theta + n\pi) = A_f \cos(\theta + n\pi - \phi_f) + A_{1/n} \cos\left(\frac{1}{n}(\theta + n\pi) - \frac{1}{n}\phi_{1/n}\right)$$
$$= (-1)^n A_f \cos(\theta - \phi_f) - A_{1/n} \cos\left(\frac{1}{n}\theta - \frac{1}{n}\phi_{1/n}\right). \tag{4.17}$$

When n is odd, $C_L(\theta + n\pi) = -C_L(\theta)$, the nth lock-on exists.

In equation (4.1), the response phase of $\frac{1}{2}S_f$ is $\frac{1}{2}\theta - \frac{1}{2}\phi_{1/2}$ at the forcing phase θ in the secondary superharmonic excitation. After one forcing period ($\Delta\theta = 2\pi$), the forcing phase returns to θ. However, if the secondary lock-on occurs, the response phase is $\frac{1}{2}\theta + \pi - \frac{1}{2}\phi_{1/2}$. This brings forth the opposite response phase at the same forcing phase. For the tertiary excitation, the response phase of $\frac{1}{3}S_f$ in equation (3.1) is $\frac{1}{3}\theta + \pi - \frac{1}{3}\phi_{1/3}$ for the forcing phase $\theta + 3\pi$. This suggests that the system has the opposite response phase at the opposite forcing phase. The response phase of $(1/n)S_f$ is $\frac{1}{n}\theta + \pi - \frac{1}{n}\phi_{1/n}$ at the forcing phase $\theta + n\pi$ after the $\frac{1}{2}n$ forcing periods. When n is even (odd), the forcing phases are the same (opposite) at the opposite response phase. Accordingly, if the secondary lock-on exists, the flows are no longer repeated in a π out-of-phase fashion. The vortex shedding pattern in the upper side is not the same as in the lower side after half of the shedding period.

5. Conclusions

Detailed numerical analyses have been performed to look into the response to superharmonic excitation in forced wakes. A direct numerical simulation has been used to portray the unsteady dynamics of wake flows behind a circular cylinder. The Reynolds number based on the diameter is $Re = 106$ and excitation is given by the rotational oscillation of the circular cylinder. The natural shedding frequency is $St_0^* = 0.168$ and the forcing frequency (S_f) varies in the vicinity of $2St_0^* = 0.336$ and $3St_0^* = 0.504$. The maximum rotation velocity (Ω_{max}) is in the range $0.10 \leqslant \Omega_{max} \leqslant 0.40$.

When the forcing frequency is about three times the natural shedding frequency, the lock-on is clearly observed. The shedding frequency (St_0) coincides with one third of the forcing frequency, i.e. the $\frac{1}{3}$ subharmonic lock-on occurs. The lift coefficient C_L is described in terms of the forcing frequency (S_f) and its subsequent shedding frequency ($\frac{1}{3}S_f$). The phase of shedding frequency ($\phi_{1/3}$) changes significantly over a small change of S_f, which is caused by the phase change of vortex shedding relative to the cylinder motion. This is similar to the case of primary lock-on. However, the maximum phase of average C_L, i.e. the phase of forcing frequency (ϕ_f) is not substantially changed. In the vorticity contours, three vortices are formed from each shoulder of the cylinder over three forcing periods. Only one vortex among them is convected in the far downstream. Once one vortex is created, a low-pressure region emerges to balance its centrifugal force. The cylinder is then forced to the direction where the vortex evolves. Between the two larger vortices, a small vortex is generated in the opposite side, which yields a small decrease of C_L.

In the secondary superharmonic excitation, modulated oscillations are observed, i.e. the secondary lock-on does not exist. The modulated oscillations are originated by the phase-variation of the $\frac{1}{2}S_f$ frequency ($\phi_{1/2}$). Since the non-phase-locked $\phi_{1/2}$ induces the discrepancy between St_0 and $\frac{1}{2}S_f$, the shedding frequencies (St_0) are not concentrated at half of the forcing frequency $\frac{1}{2}S_f$. As Ω_{max} increases, St_0 is gradually shifted from the natural shedding frequency (St_0^*) to lower frequencies. The influence of S_f on the strength of the shedding vortex is not substantial. Because of the non-occurrence of the secondary lock-on, the vortex formation and shedding patterns are variant from cycle to cycle. The near-wakes exhibit the quasi-periodic state in the secondary superharmonic excitation, which is different from the lock-on in the tertiary superharmonic excitation.

The non-occurrence of the secondary lock-on can be elucidated by analysing the relation between the forcing phase and its response phase. When the lock-on exists, the system should have the opposite response phase at the opposite forcing phase. The response phase of $(1/n)S_f$ is $\frac{1}{n}\theta + \pi - \frac{1}{n}\phi_{1/n}$ at the forcing phase $\theta + n\pi$ after the $\frac{1}{2}n$ forcing periods. When n is even (odd), the forcing phases are the same (opposite) at the opposite response phase. Accordingly, the nth lock-on exists.

This work was supported by a grant from the National Research Laboratory of the Ministry of Science and Technology, Korea.

REFERENCES

Baek, S.-J. & Sung, H. J. 1998 Numerical simulation of the flow behind a rotary oscillating circular cylinder. *Phys. Fluids* **10**, 869.

Baek, S.-J. & Sung, H. J. 2000 Quasi-periodicity in the wake of rotationally oscillating cylinder. *J. Fluid Mech.* **408**, 275.

Bearman, P. W. 1984 Vortex shedding from oscillating bluff bodies. *Ann. Rev. Fluid Mech.* **16**, 195.

Blackburn, H. M. & Henderson, R. D. 1999 A study of two-dimensional flow past an oscillating cylinder. *J. Fluid Mech.* **385**, 255.

Choi, H., Moin, P. & Kim, J. 1992 Turbulent drag reduction: studies of feedback control and flow over riblets. *Rep.* TF-55. Department of Mechanical Engineering, Stanford University, Stanford, CA.

Choi, H., Moin, P. & Kim, J. 1993 Direct numerical simulation of turbulent flow over riblets. *J. Fluid Mech.* **255**, 503.

Dennis, S. C. R., Nguyen, P. & Kocabiyik, S. 2000 The flow induced by a rotationally oscillating and translating circular cylinder. *J. Fluid Mech.* **407**, 123.

El-Refaee, M. M. 1995 Vortex lock-on for a rotationally oscillating circular cylinder – a BEM numerical study. *Engng Anal. Bound. Elem.* **15**, 235.

Fey, U., König, M. & Eckelmann, H. 1998 A new Strouhal–Reynolds-number relationship for the circular cylinder in the range $47 < Re < 2 \times 10^5$. *Phys. Fluids* **10**, 1547.

Filler, J. R., Marston, P. L. & Mih, W. C. 1991 Response of the shear layers separating from a circular cylinder to small-amplitude rotational oscillations. *J. Fluid Mech.* **231**, 481.

Griffin, O. M. & Hall, M. S. 1991 Review – vortex shedding lock-on and flow control in bluff body wakes. *Trans. ASME* I: *J. Fluids Engng* **113**, 526.

Gu, W., Chyu, C. & Rockwell, D. 1994 Timing of vortex formation from an oscillating cylinder. *Phys. Fluids* **6**, 3677.

Hover, F. S., Techet, A. H. & Triantafyllou, M. S. 1998 Forces on oscillating uniform and tapered cylinders in crossflow. *J. Fluid Mech.* **363**, 97.

Karniadakis, G. E. & Triantafyllou, G. S. 1989 Frequency selection and asymptotic states in laminar wakes. *J. Fluid Mech.* **199**, 441.

Koopman, G. H. 1967 The vortex wakes of vibrating cylinders at low Reynolds numbers. *J. Fluid Mech.* **28**, 501.

Lin, J.-C. & Rockwell, D. 1997 Quantitative interpretation of vortices from a cylinder oscillating in quiescent fluid. *Exps. Fluids* **23**, 99.

Ongoren, A. & Rockwell, D. 1988 Flow structure from an oscillating cylinder. Part 1. Mechanisms of phase shift and recovery in the near wake. *J. Fluid Mech.* **191**, 197.

Ott, E. 1993 *Chaos in Dynamical Systems*. Cambridge University Press.

Park, D. S., Ladd, D. M. & Hendricks, E. W. 1994 Feedback control of von Kármán vortex shedding behind a circular cylinder at low Reynolds numbers. *Phys. Fluids* **6**, 2390.

Pauley, L. P., Moin, P. & Reynolds, W. C. 1990 The structure of two-dimensional separation. *J. Fluid Mech.* **220**, 397.

Rockwell, D. 1998 Vortex-body interactions. *Ann. Rev. Fluid Mech.* **30**, 199.

Sheridan, J., Carberry, J., Lin, J.-C. & Rockwell, D. 1998 On the near-wake topology of an oscillating cylinder. *J. Fluids Struct*. **12**, 215.

Stansby, P. K. 1976 The locking-on of vortex shedding due to the cross-stream vibration of circular cylinders in uniform and shear flows. *J. Fluid Mech.* **74**, 641.

Techet, A. H., Hover, F. S., & Triantafyllou, M. S. 1998 Vortical patterns behind a tapered cylinder oscillating transversely to a uniform flow. *J. Fluid Mech.* **363**, 79.

Tokumaru, P. T. & Dimotakis, P. E. 1991 Rotary oscillation control of a cylinder wake. *J. Fluid Mech.* **224**, 77.

Williams, D. R., Mansy, H. & Amato, C. 1992 The response and symmetry properties of a cylinder wake subjected to localized surface excitation. *J. Fluid Mech.* **234**, 71.

Williamson, C. H. K. 1989 Oblique and parallel modes of vortex shedding in the wake of a circular cylinder at low Reynolds numbers. *J. Fluid Mech.* **206**, 579.

Williamson, C. H. K. 1996 Vortex dynamics in the cylinder wake. *Ann. Rev. Fluid Mech.* **28**, 477.